MOLECULAR IMAGING AND BIOLOGY

Mol Imaging Biol (2011)
DOI: 10.1007/s11307-011-0473-7

BRIEF ARTICLE

Targeted Multifunctional Multimodal Protein-Shell Microspheres as Cancer Imaging Contrast Agents

Renu John,[1] Freddy T. Nguyen,[1,2,3] Kenneth J. Kolbeck,[2] Eric J. Chaney,[1] Marina Marjanovic,[1] Kenneth S. Suslick,[1,2] Stephen A. Boppart[1,3,4,5,6]

[1]*Beckman Institute for Advanced Science and Technology, University of Illinois at Urbana-Champaign, 405 North Mathews Avenue, Urbana 61801, IL, USA*
[2]*Department of Chemistry, University of Illinois at Urbana-Champaign, 505 South Mathews Avenue, Urbana 61801, IL, USA*
[3]*Medical Scholars Program, University of Illinois at Urbana-Champaign, 506 South Mathews Avenue, Urbana 61801, IL, USA*
[4]*Department of Electrical and Computer Engineering, University of Illinois at Urbana-Champaign, 1406 West Green Street, Urbana 61801, IL, USA*
[5]*Department of Bioengineering, University of Illinois at Urbana-Champaign, 1304 West Springfield Avenue, Urbana 61801, IL, USA*
[6]*Department of Internal Medicine, College of Medicine, University of Illinois at Urbana-Champaign, 506 South Mathews Avenue, Urbana 61801, IL, USA*

Abstract

Purpose: In this study, protein-shell microspheres filled with a suspension of iron oxide nanoparticles in oil are demonstrated as multimodal contrast agents in magnetic resonance imaging (MRI), magnetomotive optical coherence tomography (MM-OCT), and ultrasound imaging. The development, characterization, and use of multifunctional multimodal microspheres are described for targeted contrast and therapeutic applications.

Procedures: A preclinical rat model was used to demonstrate the feasibility of the multimodal multifunctional microspheres as contrast agents in ultrasound, MM-OCT and MRI. Microspheres were functionalized with the RGD peptide ligand, which is targeted to $\alpha_v\beta_3$ integrin receptors that are over-expressed in tumors and atherosclerotic lesions.

Results: These microspheres, which contain iron oxide nanoparticles in their cores, can be modulated externally using a magnetic field to create dynamic contrast in MM-OCT. With the presence of iron oxide nanoparticles, these agents also show significant negative T2 contrast in MRI. Using ultrasound B-mode imaging at a frequency of 30 MHz, a marked enhancement of scatter intensity from *in vivo* rat mammary tumor tissue was observed for these targeted protein microspheres.

Conclusions: Preliminary results demonstrate multimodal contrast-enhanced imaging of these functionalized microsphere agents with MRI, MM-OCT, ultrasound imaging, and fluorescence microscopy, including *in vivo* tracking of the dynamics of these microspheres in real-time using a high-frequency ultrasound imaging system. These targeted oil-filled protein microspheres with the capacity for high drug-delivery loads offer the potential for local delivery of lipophilic drugs under image guidance.

Correspondence to: Stephen A. Boppart; *e-mail:* boppart@illinois.edu

Published online: 05 February 2011

Key words: Magnetomotive optical coherence tomography, Ultrasound imaging, Magnetic resonance imaging, Contrast agents, Protein microspheres, Iron oxide, RGD peptide, Alpha(v) beta(3) targeting

Introduction

Recent trends in the field of biomedical imaging have shown growing interest in and development of multimodal imaging techniques as potential tools for early detection, diagnosis, and evaluating the progression and/or response to therapy of various diseases like cancer [1, 2]. Contrast agents play an important role in improving the sensitivity of detection [3–5]. By functionalizing and targeting these agents to specific cell and molecular sites, their detection and spatial localization through imaging techniques adds molecular specificity. The potential of molecular optical imaging therefore becomes great, providing morphological, spatial, and functional information at the molecular level [6].

Optical coherence tomography (OCT) is an emerging high-resolution biomedical diagnostic imaging technology [7–11]. OCT is analogous to high-frequency ultrasound B-mode imaging except reflections of low-coherence light is detected rather than sound. This technique is attractive for medical imaging because it permits the imaging of tissue microstructure *in situ*, yielding micron-scale resolutions without the need for an invasive biopsy and histopathology. The scattering and absorption of light from tissues can be enhanced by the addition of contrast agents which are scattering in nature [3, 11–14], enabling a methodology for targeted contrast enhancement in OCT, just as there have been in other clinical imaging modalities.

A variety of contrast agents have been described in the past providing unique signatures for different imaging modalities based on different material compositions and nature of contrast [12–16]. Microbubbles filled with air or perfluorocarbon with a polyethylene glycol-phospholipid or albumin protein shell have been used as intravascular contrast agents in ultrasonography for several decades [15, 16]. The interaction of the ultrasound waves with the micron-sized gas-filled microbubbles creates echoes that enhance the contrast of ultrasound imaging. We have previously reported the use of oil-filled protein microspheres for targeting applications and as contrast agents in OCT [3, 17–20]. By incorporating superparamagnetic iron oxide nanoparticles into the core of these protein microspheres, we can achieve another level of contrast by dynamically modulating these iron oxide protein microspheres [17, 18, 20]. Magnetomotive optical coherence tomography (MM-OCT) is a novel method for imaging a distribution of magnetic contrast agents in biological specimens [18, 20–24]. This technique relies on the dynamic contrast generated through the magnetomotion of the paramagnetic contrast agents triggered by an externally modulating magnetic field. The dynamic magnetomotion of paramagnetic contrast agents results in physical nanometer-scale displacements within tissues, thereby changing the optical scattering properties of the local tissue microenvironment under observation. A phase-resolved OCT system can effectively detect the resulting increase in contrast due to magnetomotion of scatterers.

The development of targeted contrast agents has extended the scope of ultrasound-based imaging to visualize molecules and cellular processes based on the principle of accumulation of the contrast agents at specific molecular sites. However, the interaction of ultrasound with the lipid and oil shells of microbubbles and microspheres is a field of active research and medical interest owing to applications in ultrasound-mediated drug delivery. The sonification of biological tissues after the injection of intravascular microbubbles could lead to the rapid disintegration of microbubbles due to increases in acoustic pressures inside the bubble. The potential for the *in vivo* rupture of microbubbles and the release of its shell or core contents is another promising application for these agents as a means for drug administration and delivery of genetic material and proteins. Unger et al. [25] demonstrated that it was possible to incorporate hydrophobic drugs in the shells of lipid microbubbles by simply adding them to the lipid phase prior to bubble preparation. However, the use of gas-filled monolayer-based lipid microbubbles is not the most beneficial for drug delivery of most hydrophobic pharmaceutical entities because the amount of drug carried in such a bubble preparation is quite limited. The thin shell (few nanometers) restricts the loading capacity, and it may not prevent leakage of drugs from the bubble during their circulation through non-targeted areas of the body. Preparation of lipid shells with an oil phase and a hydrophobic fat-soluble drug, such as paclitaxel dissolved in the core, is another strategy [26].

Integrin receptors play an important role in angiogenesis and cancer metastasis, and targeting cells that overexpress these receptors is a promising strategy. Among the various integrin receptors, $\alpha_v\beta_3$ is known to be highly overexpressed in cancer sites and tumor vasculatures [27–29]. It has also been found that these integrin receptors play an important role in the development of atherosclerotic lesions and cardiovascular diseases. The arginine-glycine-aspartate (RGD) tri-peptide sequence has been widely used to target the $\alpha_v\beta_3$ integrin receptors [30]. Functionalization of protein microspheres with the RGD peptide ligand (KKKKKKRGD) has been tested previously on HT29 cell lines that over-express the integrin receptors [18, 19].

In this brief communication, we propose a novel microsphere-based contrast agent platform with multimodal *in*

vivo imaging and multifunctional capabilities for efficient targeted contrast enhancement and therapy. We report the synthesis of functionalized protein microspheres that are targeted to integrin receptors using the RGD ligand. These RGD microspheres have been previously shown to target the $\alpha_v\beta_3$ integrin, which is also over-expressed in rat mammary tumor models [18]. These microspheres encapsulate superparamagnetic iron oxide nanoparticles in their core, making them multimodal contrast agents in ultrasound, MM-OCT, and magnetic resonance imaging (MRI). We demonstrate *in vivo* ultrasound imaging of these target-specific agents in a preclinical mammary tumor model, as well as *in vivo* MRI. *Ex vivo* MM-OCT of excised internal organs shows accumulation of the microspheres in the tumor. These targeted protein microspheres would serve as potential site-specific drug-delivery vehicles with a high drug payload capacity.

Materials and Methods

Preparation of Targeted Iron Oxide-Containing Protein Microspheres

The protein microspheres consist of a hydrophobic core composed of vegetable oil and a hydrophilic protein shell made of bovine serum albumin (BSA). Iron oxide nanoparticles (20–30 nm) and a fluorescent dye (Nile red) have been incorporated into the core by mixing them with vegetable oil. An optimum size range of 2–5 μm has been found suitable for injection into the circulatory system. The encapsulation process is mediated through sonication using high-frequency ultrasound using a sonication apparatus (Fig. 1a). The protein shell is cross-linked through the reduction of disulfide bonds by the radicals formed during the sonication process [17–19]. Figure 1b illustrates a schematic representation of the protein microspheres.

The ferrofluid constituting the core of the microsphere was prepared by dissolving superparamagnetic iron oxide nanoparticles of size 20 to 30 nm (62.5 mg/mL) and Nile red (NR; 1.5 mg/mL) in vegetable oil. A layer of this NR-iron oxide- vegetable oil mixture was added over a 5% aqueous solution of BSA at a pH of 7.4 in the ratio 1:3 (oil/protein) in the reaction vessel. Ultrasound was applied to the oil-BSA interface at a frequency of 20 kHz using a 1-cm diameter acoustic horn at an acoustic power of 35 W/cm^2. The reaction vessel was kept in a temperature controlled bath at 45°C to prevent the denaturation of proteins. The size of the microspheres was controlled by adding surfactants to the BSA to change the effective surface tension between the oil and water phases. This step is followed by repeated washing in cold PBS buffer solution and centrifuging of the microspheres to remove excess reagents. Using an appropriate filter, microspheres under 5 μm were filtered and re-suspended in the buffer solution.

A layer-by-layer (LBL) adhesion technique was then used to modify the surface of the protein micrsospheres. This technique is

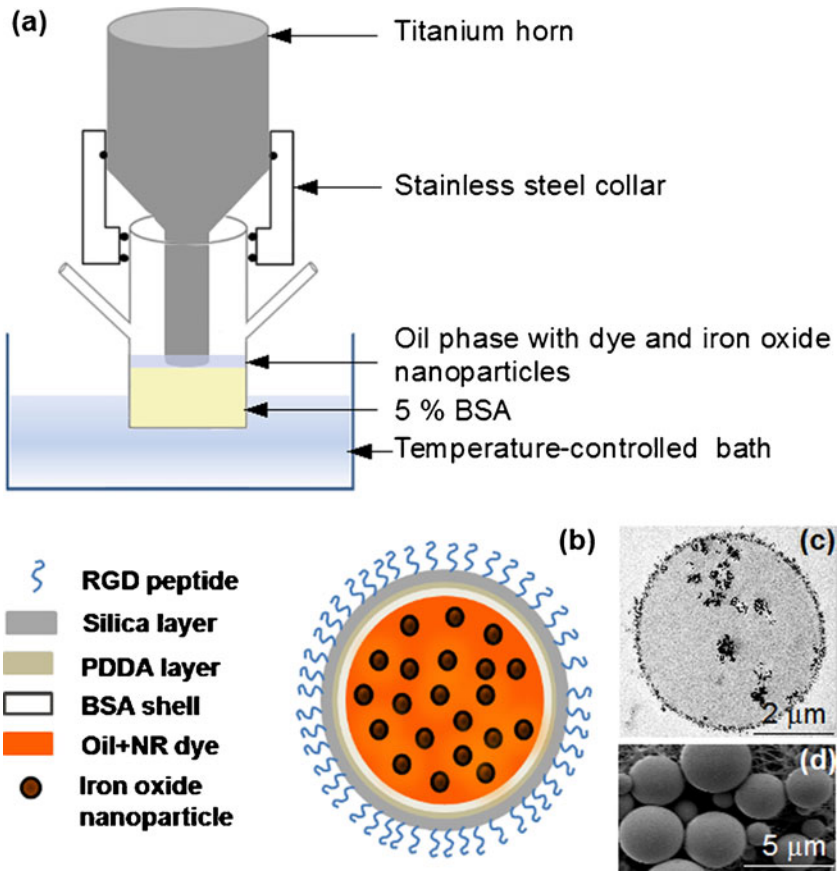

Fig. 1. Multimodal multifunctional protein-shell microspheres. **a** Sonication apparatus for the synthesis of protein microspheres. **b** Schematic representation, **c** TEM, and **d** SEM of protein microspheres.

used to functionalize the outer surface of the protein microsphere with RGD peptide sequence. Initially, a layer of PDDA polymer was added to the surface of microspheres, followed by a layer of silica. After this layer, the RGD peptide ligand was added to the outer surface. The original stock of microsphere solution was diluted to 10^8 per mL before starting the LBL adhesion process, for best results. Then, 1 mL of cold PDDA solution at 1 mg/mL was added to the microspheres and the suspension was kept on a rotisserie stage for 30 min in a refrigerator. After the PDDA adhesion, the microspheres were spun down and the subnatant solution was removed. The microspheres were again re-suspended in 0.2 mL of PBS. The LBL step was repeated with 1 mL of 1% silica solution added to the microspheres. After the silica layering, the process was again repeated with 1 mg/mL RGD solution. This RGD peptide sequence was synthesized by the Protein Sciences Facility in the Biotechnology Center at the University of Illinois at Urbana-Champaign. The RGD functionalized Nile Red-superparamagnetic iron oxide encapsulated (RGD-NR-SPIO) protein microspheres were kept on the rotisserie in the refrigerator until they were used. These microspheres were characterized using dynamic light scattering studies, TEM and SEM (Fig. 1c, d) and found to have size distribution between 2 and 5 μm.

Experiments

To demonstrate the feasibility of the multimodal multifunctional microspheres as contrast agents in ultrasound, MM-OCT and MRI, three different female Sprague–Dawley rats (weighing ~180 g) were used. Experiments were performed under protocols approved by the Institutional Animal Care and Use Committee at the University of Illinois at Urbana-Champaign. Two normal rats were used for MRI, one served as a negative control and one was injected with iron oxide protein microspheres. One female rat with a large spontaneous mammary tumor (fibroadenoma) was used for ultrasound and MM-OCT imaging. After *in vivo* ultrasound imaging, the rat was euthanized by CO_2 inhalation, followed by resection of the tumor and various internal organs. OCT and MM-OCT were performed on the *ex vivo* tumor and internal organs. After *ex vivo* OCT and MM-OCT imaging, the tissues were placed in a freezing box containing isopropanol to control the rate of temperature decline and left at −80°C overnight. Frozen tissues were cryosectioned, with a thickness of 10 μm, using a cryostat (Leica CM 3050S). Thin cryosections were overlaid on poly-L-lysine precoated slides (Histology Control Systems, Inc.), dried at room temperature for 30 min, and fixed with cold acetone for 15 min at 4°C. These sections were used for histological processing and white-light and fluorescence microscopy.

MRI Studies

MRI was performed on two normal rats, one injected with non-targeted iron oxide protein microspheres and the other served as a negative control. A 1-mL volume (approximately 1.5×10^{10} microspheres) was injected in the tail vein of a 180 g anesthetized rat at a rate of 1 mL/h. This dose approximately corresponds to an injection of 45 mg iron oxide per kilogram body weight. The MRI was performed within 60 min after the completion of the injection on a 4.7 T (200 MHz for 1 H) SISCO/Varian NMR spectrometer (Palo Alto, CA, USA) with a 33 cm horizontal bore superconducting magnet (Oxford Instruments Ltd, Oxford, UK) equipped with a 6.5 G/cm gradient coil system. The Varian VNMR 6.1 C software was used for collecting and processing images. A spin-echo multi-slice pulse sequence was employed. The coronal and axial T2-weighted images were acquired slice by slice with no gap between slices. The repetition time was 2.5 s and echo times were varied from 11 to 50 ms. The images were acquired for a field of view of 8.0×3.5 cm^2 (coronal) and 3.5×3.5 cm^2 (axial) with in-plane resolutions of 312×273 μm^2 (coronal) and 273×273 μm^2 (axial) and a slice thickness of 1.0 mm.

Ultrasound Imaging

Ultrasound imaging was performed using a VisualSonics Vevo 2100TM system. The rat tumor (approximately 4×5 cm) was initially imaged with a 15 MHz transducer (MS200) in B-mode and with Doppler to locate a highly vascular region in the tumor. A 30 MHz transducer (MS400) was subsequently used to provide higher resolution details of this vascular region. Following localization of this vascular bed, ultrasound imaging was performed after bolus injection of 200 μL of non-targeted microbubbles (MicroMarker Contrast Agents, VisualSonics) through a tail vein. A rupture pulse sequence of multiple 10 MHz high-power pulses was used to ensure the clearance of microbubbles in circulation before the administration of protein microspheres. This was followed by bolus injection of RGD-protein microspheres and additional ultrasound imaging.

MM-OCT Imaging

MM-OCT imaging was performed *ex vivo* on the tumor and all internal organs of the rat approximately 4-h post injection of RGD-protein microspheres. A spectral-domain OCT system with a Ti:Al_2O_3 femtosecond laser (KMLabs, Inc.) was used as the light source. The femtosecond laser was pumped by a frequency-doubled Nd:YVO_4 laser (Coherent, Inc.) with 4.5 W of 532 nm light. The light with a bandwidth of 120 nm (providing ~3 μm axial resolution in tissue) centered at 800 nm light was coupled to a single-mode fiber interferometer providing ~8 mW at the sample. The sample-arm beam was scanned across the tissue using galvanometer-mounted mirrors placed one focal length above a 30 mm achromatic imaging lens (providing ~12 μm transverse resolution). A magnetic field of ~0.08 T and a gradient of ~15 T/m within the sample imaging volume were generated using a custom-made water-cooled electromagnet. The light beam on the specimen was scanned through the central bore of the solenoid. Interference between the reference and sample beams was measured with a custom-designed spectrometer composed of a grating, imaging lens, and line camera (Piranha 2, Dalsa, Inc.) providing an optical imaging depth of 2 mm and the capability of a 33 kHz line acquisition rate. The magnetic modulation frequency f_B was chosen to be around 100 Hz for the tumor tissue based on studies reported previously [21]. A lower axial scan rate of 1 kHz was chosen to avoid excessive oversampling. The camera exposure time was 250 μs. Each B-mode scan was performed over 2.5 mm of the specimen (4,000 pixels in width by 1,024 pixels in depth) with an acquisition time of 4 s. Each image was acquired twice, once with the magnetic field on and once with the field off.

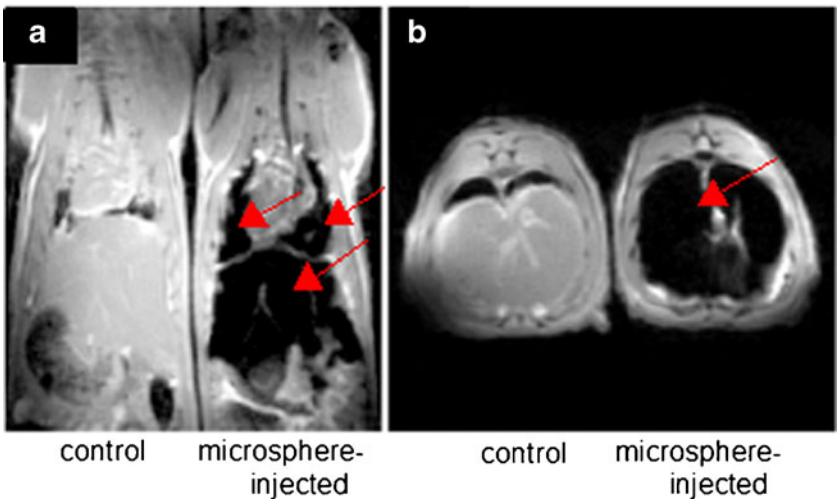

Fig. 2. **a** Coronal and **b** sagittal MRI slices of a control rat and a normal rat after injection with non-targeted iron oxide microspheres. The arrow-marked regions in the MRI, after injection of iron oxide protein microspheres, show strong negative T2 contrast due to the presence of iron oxide.

Results and Discussions

A comparison of the coronal and sagittal images from the control rat and the rat injected with microspheres (Fig. 2) shows significant differences in the liver regions of the rats, where it is known that these non-targeted microspheres accumulate. Compared to the control rat, there is a strong negative contrast enhancement in the liver of the rat injected with the microspheres due to the presence of iron oxide. The spleen also exhibits negative contrast enhancement due to the presence of the iron oxide. There was no change in contrast in tissues that do not contain large numbers of phagocytic macrophages. This clearly demonstrates that the iron oxide-loaded microspheres serve as negative T2 contrast agents in MRI.

The rat tumor was initially imaged with a 15 MHz transducer in B-mode and with Doppler to locate a highly

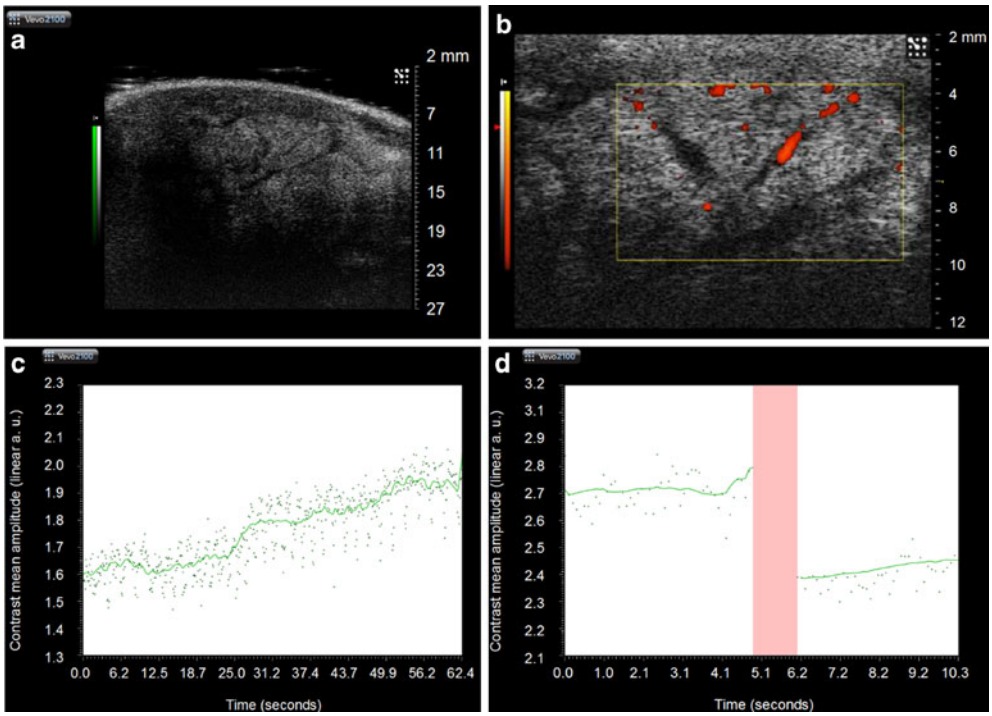

Fig. 3. High-resolution real-time *in vivo* ultrasound images of rat mammary tumor and microbubble transients. **a** Tumor imaged with 15 MHz probe. **b** Doppler flow imaging identifying vascular region. **c** Transient increase in scattering (*green trace*) following commercial microbubble injection. **d** Rapid decrease in scattering (*green trace*) following delivery of rupture pulse (*red region*).

vascular region of the tumor (Fig. 3a, b). Using ultrasound guidance, it was also possible to differentiate necrotic areas from the more highly vascularized regions at the periphery of the tumor. After the injection of microbubbles, the ultrasound images showed an increase in scattering as the non-targeted microbubbles circulated through the tumor vasculatures (Fig. 3c). On delivery of a rupture pulse sequence, the signal levels dramatically and transiently decreased (Fig. 3d). Additional rupture pulse sequences were administered to ensure the clearance of microbubbles from the circulation prior to administration of the RGD-NR-SPIO protein microspheres. While continuing the ultrasound imaging of the same region, the RGD-NR-SPIO protein microspheres were administered intravenously to the rat. Using the same ultrasound image subtraction method as used with the gas-filled microbubbles, it was possible to definitively identify the presence of our microspheres in the tumor (Fig. 4a). Ultrasound images obtained after the injection of RGD microspheres showed an increase in scattering signal, just as with the microbubbles. The dynamic scattering changes on injection of protein microspheres were unique, first increasing with the bolus, and then falling toward a new baseline scattering level (Fig. 4b). We hypothesize this occurred because as the bolus of targeted microspheres passed through the tumor, we detected the increase, but as the microspheres circulated, reached target sites, and bound within the tumor vasculature, the scattering level dropped, until the binding sites were substantially occupied, and the new scattering baseline level was established (higher than pre-injection).

Next, a series of 10 MHz high-intensity rupture pulse sequences were delivered from the instrument (Fig. 4c). This time, however, rather than a rapid decrease in scattering from ruptured microbubbles, we observed (repeatedly) a rapid transient increase in scattering before returning to

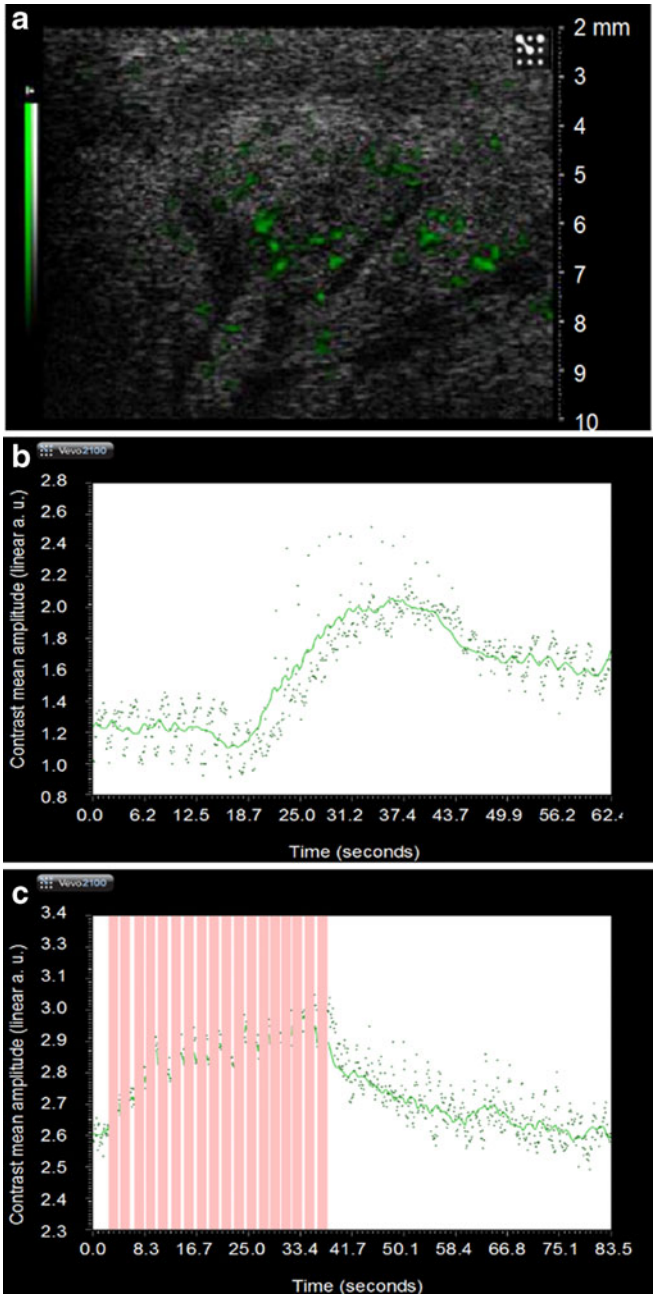

Fig. 4. High-resolution real-time ultrasound imaging of tumor following injection of engineered protein microspheres. **a** Identified microspheres (*green channel*) within tumor, superimposed over grey-scale B-mode image. **b** Transient scattering changes (*green trace*) following bolus injection. **c** Transient scattering changes (*green trace*) following a sequence of rupture pulses (*red regions*), showing increases in scattering immediately after rupture pulses, followed by a gradual decrease in scattering, suggesting possible rupture of microspheres.

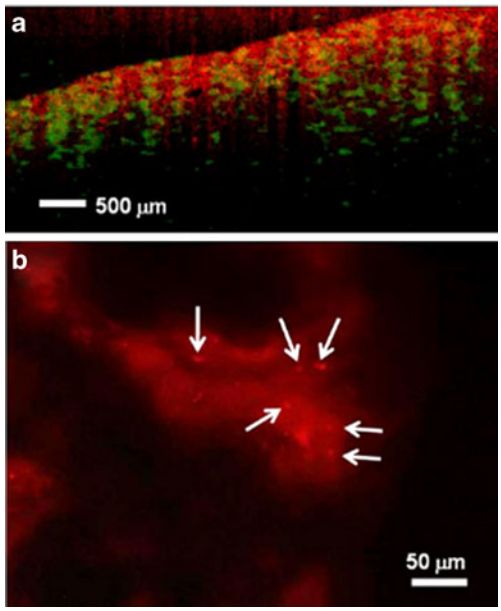

Fig. 5. Multimodal imaging of multifunctional microspheres. **a** MM-OCT image showing both magnetomotive (*green*) and structural (*red*) signals from the tumor site. **b** High-magnification (63×) fluorescence microscopy of the tumor showing intact Nile red-containing microspheres (*arrows*) as well as evidence of microsphere rupture (*diffuse red signal*).

baseline, and gradual decrease in scattering. We hypothesize that this is due to an acoustomotive excitation of the microspheres, with possible indications of rupture. We believe this may allow us to uniquely identify the presence of our microspheres, and understand the dynamics of their binding. Following repeated rupture pulse sequences, the elevated baseline level of scattering gradually decreased, but never returned to the pre-injection level even after 45 min. We hypothesize this was due to the high-affinity binding of the targeted microspheres, the rupture of some but not all of the microspheres, and their gradual detachment and clearance by the liver over time.

The magnetomotive OCT images of the tumor (Fig. 5a) showed clear magnetomotive signal from the microspheres (green channel). A weak magnetomotive signal was observed from the liver and the bladder, and a large signal was observed from the lungs (data not shown). Further investigations are underway to determine if the size or charge of these microspheres limited their ability to pass through the pulmonary circulation. Previous studies have shown the non-targeted microspheres are finally cleared through the macrophages in liver, lungs and spleen [18]. Histology was performed on the tumor tissue, at the site of imaging. Under fluorescence microscopy (Fig. 5b), using filters that allow the Nile Red fluorescence emission to be selectively imaged, there appeared to be a few intact microspheres present, as well as a more diffuse appearance of dye, likely from ruptured microspheres.

During this study, MM-OCT was perfomed *ex vivo*, approximately 4 h post injection of RGD-NR-SPIO protein microspheres. Due to time constraints and multiple users, we were unable to integrate our magnetomotive coils with the ultrasound system. However, in the future, we plan to incorporate our magnetomotive coils with the ultrasound transducer so that we could modulate the magnetic microspheres externally and detect this modulation using ultrasound B-mode imaging or Doppler ultrasound.

No information is currently available regarding the life time or clearance of these microspheres *in vivo*, nor their long term stability and viability. Our studies indicate that the iron oxide microspheres, up to 10^{11} microspheres per mL, with up to 1 mL/100 g of rat body weight, are safe for short-term studies up to 24 h. Preliminary studies showed that the non-targeted microspheres accumulate in the liver, lungs, and spleen from 15 min to few hours. However, no studies have been carried out on the long term toxicity effects or clearance time of these microspheres from the circulation and system. Studies are currently being conducted on the biodistribution, binding properties, breakdown, and clearance properties of targeted microspheres in the circulation.

Conclusions

In this feasibility study and brief communication, we have described the development, characterization, and use of multifunctional multimodal microspheres as targeted contrast and therapeutic agents. Preliminary results using a high-resolution, real-time, *in vivo*, small animal ultrasound imaging system are promising and demonstrate the potential use of the system for detecting, quantifying, and tracking the *in vivo* dynamics of our multifunctional multimodality microspheres. We have shown that these protein microspheres show negative T2 contrast enhancement in MRI. The *ex vivo* MM-OCT results show that the RGD targeted microspheres accumulate in the tumor. These preliminary results demonstrate the feasibility of using RGD-NR-SPIO protein microspheres as multi-modal contrast agents for targeting and drug-delivery applications. The *in vivo* ultrasonography and *ex vivo* fluorescence microscopy images suggest that our microspheres ruptured following the delivery of ultrasound rupture pulse sequences, which would enable these microspheres to be used as future drug-delivery vehicles in therapeutic applications in treating cancer and cardiovascular disease. Investigations are underway for incorporating lipophilic chemotherapeutic drugs, such as paclitaxel, into the oil core. Feasibility studies are also being conducted for replacing Nile Red with a suitable near IR dye to enhance the *in vivo* fluorescence imaging capabilities of the contrast agent and to study the *in vivo* whole-body biodistribution dynamics of the protein microspheres. We believe these imaging instruments and this methodology will enable us to track the effects of binding efficiency in different tumors or atherosclerotic lesions, or with different functional ligands or antibodies on the microspheres.

Acknowledgements. This research was supported in part by grants from the National Institutes of Health (Roadmap Initiative, NIBIB R21 EB005321, NIBIB R01 EB009073, and NCI RC1 CA147096).

Conflicts of Interest. Stephen A. Boppart receives royalties related to optical coherence tomography for patents licensed by the Massachusetts Institute of Technology. He is also co-founder of Diagnostic Photonics, Inc., a company developing Interferometric Synthetic Aperture Microscopy for medical applications, and he receives funding for sponsored research projects from Welch Allyn, Inc. and Samsung, Inc., related to optical imaging technologies. All other authors report no real or perceived conflicts of interest.

References

1. Wang X, Yang L, Chen Z, Shin DM (2008) Application of nanotechnology to cancer therapy and imaging. CA Cancer J Clin 58:97–110
2. Moghimi SM, Hunter AC, Murray JC (2005) Nanomedicine: current status and future prospects. FASEB J 19:311–330
3. Boppart SA, Oldenburg AL, Xu C, Marks DL (2005) Optical probes and techniques for molecular contrast enhancement in coherence imaging. J Biomed Opt 10:041208
4. Lee TM, Toublan FJ, Sitafalwalla S et al (2003) Engineered microsphere contrast agents for optical coherence tomography. Opt Lett 28:1456–1458
5. McCarthy JR, Weissleder R (2008) Multifunctional magnetic nanoparticles for targeted imaging and therapy. Adv Drug deliv Rev 60:1241–1251
6. Gao X, Gui Y, Levenson RM et al (2004) *In vivo* cancer targeting and imaging with semiconductor quantum dots. Nat Biotechnol 22:969–976
7. Huang D, Swanson EA, Lin CP et al (1991) Optical coherence tomography. Science 254:1178–1181
8. Bouma BE, Tearney GJ (eds) (2002) Handbook of Optical Coherence Tomography. Marcel Dekker, New York, New York

9. Boppart SA, Bouma BE, Pitris C et al (1998) Intraoperative assessment of microsurgery with three-dimensional optical coherence tomography. Radiology 208:81–86
10. Nguyen FT, Zysk AM, Chaney EJ et al (2009) Intraoperative evaluation of breast tumor margins with optical coherence tomography. Cancer Res 69:8790–8796
11. Rao KD, Choma MA, Yazdanfar S et al (2003) Molecular contrast in optical coherence tomography by use of a pump-probe technique. Opt Lett 28:340–342
12. Xu C, Ye J, Marks DL, Boppart SA (2004) Near-infrared dyes as contrast-enhancing agents for spectroscopic optical coherence tomography. Opt Lett 29:1647–1649
13. Oldenburg AL, Hansen MN, Zweifel DA et al (2006) Plasmon-resonant gold nanorods as low backscattering albedo contrast agents for optical coherence tomography. Opt Express 14:6724–6738
14. Cang H, Sun T, Li Z-Y et al (2005) Gold nanocages as contrast agents for spectroscopic optical coherence tomography. Opt Lett 30:3048–3050
15. Barton JK, Hoying JB, Sullivan CJ (2002) Use of microbubbles as an optical coherence tomography contrast agent. Acad Radiol 9:S52–S55
16. Rapoport N, Gao Z, Kennedy A (2007) Multifunctional nanoparticles for combining ultrasonic tumor imaging and targeted chemotherapy. J Natl Cancer Inst 99:1095–1106
17. Kolbeck KJ (1999) Biomedical applications of protein microspheres, PhD Dissertation in Chemistry. University of Illinois at Urbana-Champaign, Urbana
18. Dibbern EM (2005) Core shell microspheres for biomedical applications, PhD Dissertation, Department of Chemistry, University of Illinois at Urbana-Champaign, Urbana, Illinois
19. Toublan FJJ, Boppart SA, Suslick KS (2006) Tumor targeting by surface-modified protein microspheres. J Am Chem. Soc.128:3472–3473
20. Oldenburg AL, Toublan FJ, Suslick KS et al (2005) Magnetomotive contrast for *in vivo* optical coherence tomography. Opt Express 13:6597–6614
21. Oldenburg AL, Gunther JR, Boppart SA (2005) Imaging magnetically labeled cells with magnetomotive optical coherence tomography. Opt Lett 30:747–749
22. Oldenburg AL, Crecea V, Rinne SA, Boppart SA (2008) Phase-resolved magnetomotive OCT for imaging nanomolar concentrations of magnetic nanoparticles in tissues. Opt Express 16:11525–11539
23. John R, Chaney EJ, Boppart SA (2010) Dynamics of magnetic nanoparticle-based contrast agents in tissues tracked using magnetomotive optical coherence tomography. IEEE J Sel Top Quantum Electron 16:691–697
24. John R, Rezaeipoor R, Adie SG et al (2010) *In vivo* magnetomotive optical molecular imaging using targeted magnetic nanoprobes. Proc Natl Acad Sci USA 107:8085–8090
25. Unger EC, McCreery TP, Sweitzer RH (1998) A novel ultrasound contrast agent with therapeutic properties. Acad Radiol 5:S247–S249
26. Unger EC, McCreery TP, Sweitzer RH et al (1998) Acoustically active lipospheres containing paclitaxel: a new therapeutic ultrasound contrast agent. Invest Radiol 33:886–892
27. Eliceiri BP, Cheresh DA (1999) The role of alpha v beta 3 integrins during angiogenesis. J Clin Invest 103:1227–1230
28. Hoshiga M, Alpers CE, Smith LL et al (1995) Alpha-v beta-3 integrin expression in normal and atherosclerotic artery. Circ Res 77:1129–1135
29. Pasqualini R, Koivunen E, Ruoslahti E (1997) α v integrins as receptors for tumor targeting by circulating ligands. Nat Biotechnol 15:542–546
30. Winter PM, Morawski AM, Caruthers SD et al (2003) Molecular imaging of angiogenesis in early-stage atherosclerosis with alpha(v) beta(3)-integrin-targeted nanoparticles. Circulation 108:2270–2274